Large hydrogen isotope fractionations distinguish nitrogenase-derived methane from other sources

Running title: Stable isotopes of nitrogenase-derived methane

Katja E. Luxem,[1,2*] William D. Leavitt,[3,4,5] Xinning Zhang[1,2*]

[1]Dept. of Geosciences, [2]Princeton Environmental Institute, Princeton University; [3]Dept. of Earth Sciences, [4]Dept. of Chemistry, [5]Dept. of Biological Sciences, Dartmouth College

***Corresponding Authors:**

Katja Luxem, kluxem@princeton.edu, (609) 258-4674

Xinning Zhang, xinningz@princeton.edu, (609) 258-2489

Department of Geosciences (M47 Guyot Hall)

Princeton University, Princeton NJ 08540

Abstract

Nitrogenase is the main source of natural fixed nitrogen for the biosphere. Two forms of this metalloenzyme, the vanadium (V) and iron (Fe)-only nitrogenases, were recently found to reduce small amounts of carbon dioxide into the potent greenhouse gas methane. Here we report carbon and hydrogen stable isotopic compositions and fractionations of methane generated by V- and Fe-only nitrogenases in the metabolically versatile nitrogen fixer *Rhodopseudomonas palustris*. The stable carbon isotope fractionation imparted by both forms of alternative nitrogenase are within the range observed for hydrogenotrophic methanogenesis ($^{13}\alpha_{CO2/CH4}$ = 1.051 ± 0.002 for V-nitrogenase and 1.055 ± 0.001 for Fe-only nitrogenase, mean ± SE). In contrast, the hydrogen isotope fractionations ($^{2}\alpha_{H2O/CH4}$ = 2.071 ± 0.014 for V-nitrogenase and 2.078 ± 0.018 for Fe-only nitrogenase) are the largest of any known biogenic or geogenic pathway. The large $^{2}\alpha_{H2O/CH4}$ shows that the reaction pathway nitrogenases use to form methane strongly discriminates against ^{2}H, and that $^{2}\alpha_{H2O/CH4}$ distinguishes nitrogenase-derived methane from all other known biotic and abiotic sources. These findings on nitrogenase-derived methane will help constrain carbon and nitrogen flows in microbial communities and the role of the alternative nitrogenases in global biogeochemical cycles.

Importance

All forms of life require nitrogen for growth. Many different kinds of microbes living in diverse environments make inert nitrogen gas from the atmosphere bioavailable using a special protein, *nitrogenase*. Nitrogenase has a wide substrate range, and in addition to producing bioavailable nitrogen, some forms of nitrogenase also produce small amounts of the greenhouse gas methane. This is different from other microbes that produce methane to generate energy. Until now, there

was no good way to determine when microbes with nitrogenases are making methane in nature. Here, we developed an isotopic fingerprint that allows scientists to distinguish methane from microbes making it for energy versus those making it as a byproduct of nitrogen acquisition. With this new fingerprint, it will be possible to improve our understanding of the relationship between methane production and nitrogen acquisition in nature.

Introduction

Microorganisms produce over half of global methane emissions (1). Fermentative and hydrogenotrophic methanogens are the most significant microbial producers of this potent greenhouse gas (1, 2). Their metabolic pathways occur exclusively within anaerobic Archaea and involve multiple enzymes working together in series, including the obligatory methyl-coenzyme M reductase (*mcr*) enzyme. Its primary function is for catabolism, with methane production thought to occur only after other more favorable electron acceptors, like oxygen, nitrate, or sulfate have been consumed (3–5). Over the past decade, it has been recognized that minor additional contributions of methane derive from the demethylation of organophosphonates (c.f. (6–8)) and from inefficient Wood-Ljungdahl pathway carbon fixation (9). Most recently, it was discovered that some forms of the metalloenzyme nitrogenase also reduce carbon dioxide straight into methane (10). Nitrogenases are the only biological source of newly fixed nitrogen to the biosphere, and prior to industrial reduction of dinitrogen, were the primary source of nitrogen to life on Earth (11, 12). The discovery of biological methane production by nitrogenase expands the known range of organisms and environments in which methane production is possible.

Nitrogenase is known primarily for its ability to reduce inert dinitrogen (N_2) gas into ammonia, a process known as nitrogen fixation. This biological nitrogen source plays a critical role in ecosystem fertility. Nitrogenase is generally considered a promiscuous enzyme because it can reduce a variety of carbon containing compounds in addition to N_2 (13–17). For example, the iron (Fe)-only nitrogenase isoform can convert carbon monoxide into hydrocarbon chains, a reaction which may have been important for early forms of life (15). In addition, all forms of nitrogenase reduce acetylene to ethylene (18–21), which is the basis for the most commonly used acetylene reduction method to measure nitrogen fixation rates in the laboratory and field (22–

24). The recent discovery that some forms of nitrogenase can reduce carbon dioxide to methane (10) is significant because, unlike acetylene and carbon monoxide, carbon dioxide is ubiquitous in nature.

The vanadium (V-) and Fe-only nitrogenase isoforms, which were shown to produce the most byproduct methane of the various nitrogen isoforms (10), are found in both the bacterial and archaeal domains and are widespread in nature (25–30). In addition, certain artificial mutations near the active site of the molybdenum (Mo)-nitrogenase enabled this more common isoform to produce methane (31, 32). These findings beg the question of whether and to what extent nitrogenase is an important methane source in certain environments, and how to distinguish nitrogenase-derived methane from other sources. Previous research has established that each form of nitrogenase imparts a characteristic nitrogen or carbon isotope fractionation during N_2 (33) or acetylene (26) reduction, respectively. The stable isotopes of carbon and hydrogen are commonly used to differentiate ('fingerprint') different sources of methane (2, 8, 34–39). To determine what characteristic carbon and hydrogen isotope fractionations are associated with methane production by the different nitrogenases, we cultivated V- and Fe-nitrogenase utilizing strains of the anoxygenic photoheterotroph *Rhodopseudomonas palustris* under nitrogen-fixing conditions. We find that the carbon isotope fractionations are large, yet similar to those of canonical anaerobic methanogens. Conversely, the hydrogen isotope fractionation values are the largest of any methane production pathway on record. This unique hydrogen isotopic fingerprint allows us to differentiate nitrogenase-derived methane from other sources, and provides insight into the mechanism of proton delivery to nitrogenase.

Results and Discussion

Isotope fractionation by nitrogenase during methane production

Different methane sources are commonly associated with characteristic stable isotope fractionations that can help distinguish between different biogenic, geogenic and thermogenic sources (2, 36, 39). To determine the stable isotopes associated with methane production by nitrogenase, we grew mutant strains of the anoxygenic photoheterotroph *Rhodopseudomonas palustris* CGA009 that exclusively utilize either the Mo-nitrogenase, V-nitrogenase or Fe-only nitrogenase for nitrogen fixation (10, 40, 41). The Mo-nitrogenase strain did not produce detectable methane during batch culture incubation through stationary phase in Balch tubes (data not shown). The V- and Fe-only nitrogenase strains both produced methane, with the Fe-only nitrogenase strain producing over an order of magnitude more methane than the V-nitrogenase strain (Fig. 1). For the Fe-nitrogenase strain, methane production per cell was higher later during growth. We measured the carbon and hydrogen isotopic compositions of methane and fractionations relative to carbon dioxide (CO_2/CH_4) and water (H_2O/CH_4), as produced by the V- and Fe-only nitrogenases across a range of cell densities (OD_{660} ~ 0.3 to 1.3, from early log to stationary phase), temperatures (14 to 30°C), carbon substrates (succinate and acetate), and growth medium pH (from 6.2 to 6.8 at inoculation).

We discovered that methane produced by the V- and Fe-only nitrogenases is highly depleted in deuterium relative to other natural sources (Fig. 2). Growth on medium with substrate water δ^2H of ~ −40‰ yielded methane with δ^2H values ranging from −473 to −560‰. To our knowledge, this is the most deuterium-depleted hydrogen isotope ratio measured for natural methane sources to date. The methane carbon isotopic composition, which varied from $\delta^{13}C$ = −73.0 to −97.1‰

for substrate CO_2 of ~ −30‰, falls within the range observed for hydrogenotrophic methanogenesis (2) but is distinct from other abiogenic (36) and non-traditional biotic sources (8).

Attributing methane isotope ratios to specific pathways becomes more reliable when the isotopic composition of source water and carbon are also considered (34, 36). In our experiments, manipulation of growth medium δ^2H over a ~ 600‰ range, from −30 to 550‰, resulted in a constant, statistically indistinguishable fractionation of $^2\alpha_{H2O/CH4} = (\delta^2H_{H2O}+1000)/(\delta^2H_{CH4}+1000) = 2.047 \pm 0.016$ calculated for individual samples, $^2\alpha_{H2O/CH4} = 2.056 \pm 0.057$ calculated using the slope, and $^2\alpha_{H2O/CH4} = 2.050 \pm 0.019$ calculated using the intercept ($p = 0.9$; Fig. 3). The hydrogen isotope fractionations ($1.820 \leq {}^2\alpha_{H2O/CH4} \leq 2.199$) measured for methane production by V- and Fe-only nitrogenase over a range of temperatures and growth conditions are substantially higher than the largest fractionations observed for traditional microbial methanogenesis pathways, which are around $^2\alpha_{H2O/CH4}$ ~1.45 for acetoclastic (42) and hydrogenotrophic (34) methanogenesis (Figs. 4A, 5). In fact, depending on the substrate concentrations and environmental conditions like temperature, the hydrogen isotope fractionation for these traditional methane-forming pathways is often even lower than $^2\alpha_{H2O/CH4}$ =1.45 (34, 42, 43). Our data indicate that a large hydrogen isotope fractionation of $^2\alpha_{H2O/CH4}$ ~ 2.070 is characteristic of methane production by nitrogenase and distinguishes methane produced by nitrogenase from other biogenic and abiogenic pathways.

Like the carbon isotopic composition, the carbon isotope fractionation measured for nitrogenase ($1.045 \leq {}^{13}\alpha_{CO2/CH4} = (\delta^{13}C_{CO2}+1000)/(\delta^{13}C_{CH4}+1000) \leq 1.062$) falls within the range observed

for hydrogenotrophic methanogenesis ($1.030 \leq {}^{13}\alpha_{CO2/CH4} \leq 1.080$; (37); Fig. 4B). Mechanistically, it is possible that the similarity in carbon isotope fractionation between these two pathways is due to the similarity in substrate (CO_2) and electron requirements.

We observed only small changes in nitrogenase fractionation across a large range of temperatures, cell densities, and carbon substrates (<0.02 for ${}^{13}\alpha_{CO2/CH4}$ and < 0.38 for ${}^{2}\alpha_{H2O/CH4}$; Figs. 4, 5) relative to the variability observed for other methane production pathways. Fractionation increased by ~ 0.012 as temperature decreased from 30 to 14°C for ${}^{13}\alpha_{CO2/CH4}$ ($p = 10^{-5}$) and by ~ 0.160 for ${}^{2}\alpha_{H2O/CH4}$ ($p = 0.03$). In contrast, the form of growth substrate (succinate or acetate) did not alter ${}^{2}\alpha_{H2O/CH4}$ ($p = 0.96$) and only had a small impact of ~0.005 on ${}^{13}\alpha_{CO2/CH4}$ ($p = 0.006$). This is compatible with the recent observation that electron availability has only a minor impact on CH_4 production by a mutant Mo-nitrogenase isoform (44). Acidification of the growth medium by ~0.5 pH units also did not alter fractionation, though we note that there was only one biological replicate for the acidified treatment (Table 1). Despite order of magnitude differences in the rate of methane production by V- and Fe-only nitrogenase (Fig. 1), they have indistinguishable fractionation factors associated with methane production ($p = 0.4$ for ${}^{13}\alpha_{CO2/CH4}$ and 0.9 for ${}^{2}\alpha_{H2O/CH4}$; Table 1). This suggests there is no rate effect on fractionation and that the V- and Fe-only nitrogenases share a common mechanism for CO_2 reduction to methane.

The greatest source of variability in fractionation (${}^{13}\alpha_{CO2/CH4}$ ~ 0.01; ${}^{2}\alpha_{H2O/CH4}$ ~ 0.25 range) appears to be due to cell density, growth phase (Figs. 5C, G), or substrate (CO_2) concentration (Figs. 5D, H). These variables are strongly correlated due to dissolved inorganic carbon (DIC) production throughout growth (Fig. 5I) and cannot be disentangled with the current dataset.

Future experiments could manipulate the DIC concentration to test the mechanistic basis for this effect. Notably, a similar cell density or growth phase effect has been previously observed for anaerobic methanogenesis, where it was tentatively attributed to changes in temperature, catabolic rate (42) or carbon assimilation during logarithmic growth (45).

The methane isotopic composition at harvest integrates the isotopic composition of methane produced throughout growth. Therefore, the fractionation measured at stationary phase is altered by the change observed in substrate CO_2 isotopic composition during exponential phase (Fig. 5J). However, using the observed shift in medium CO_2 isotopic composition to estimate the effect on the fractionation measured at stationary phase, we find that the change in substrate isotopic composition could account for at most half (~0.005) of the total (~0.01) shift observed in $^{13}\alpha_{CO2/CH4}$ with cell density (see S.I.). We note that it is possible that the isotopic composition of intracellular CO_2 is somewhat different from the bulk composition due to localized production, consumption, and depletion, given the competing reactions of CO_2 production during organic substrate assimilation and re-fixation by Rubisco during photoheterotrophic growth of *R. palustris* (41, 46, 47).

We observed changes in fractionation correlated with temperature, growth phase and dissolved inorganic carbon (DIC) concentration but not with organic carbon substrate or total methane production rate. Though the variability in fractionation during methane production by nitrogenase is interesting from a mechanistic perspective, the range of measured hydrogen isotope fractionation does not overlap with, and is readily distinguishable from, the range observed for other methane production pathways (Fig. 4). This is consistent with the observation

that N_2 and acetylene (C_2H_2) fractionations by a single nitrogenase isoform are also remarkably constant across different organisms, metabolisms and environmental conditions (26, 33).

Hydrogen concentration does not influence methane isotope fractionation by nitrogenase

Hydrogen (H_2) is an obligatory product of nitrogen fixation and, in our experiments, is generated simultaneously with the production of methane from carbon dioxide (48, 49). We explored whether its buildup could affect methane isotope fractionation by nitrogenase, as has been suggested for *mcr*-based methanogenesis (2, 42, 50–58). Two lines of evidence show that the presence of H_2 does not alter the isotopic composition of methane produced by nitrogenase. Firstly, for Fe-only nitrogenase cultures (grown on succinate at 19°C in serum vials), the hydrogen isotope fractionations were indistinguishable in cultures in which the headspace contained 2-3% H_2 at inoculation ($^2\alpha_{H2O/CH4}$ = 2.068 ± 0.033, n = 3) and in cultures that were flushed with 100% N_2 prior to inoculation ($^2\alpha_{H2O/CH4}$ = 2.046 ± 0.016, n = 4, p = 0.57; S.I. Table). These data show that exogenous H_2 did not influence the isotopic composition of the product methane. This result is expected given that the strains used in our experiments lack a functional uptake hydrogenase (59) and that nitrogenase itself does not catalyze isotope exchange between water and H_2 (60). (This is a significant distinction from the hydrogenation of D_2, forming HD, which nitrogenase ***can*** catalyze in the presence of N_2). We note that abiotic hydrogen isotopic equilibration between H_2-H_2O, CH_4-H_2 and CH_4-H_2O is likely too slow to be important at the timescales (~weeks) and temperatures (≤ 30°C) of relevance to our experiments (36, 61–63). This finding is consistent with other reports that the source of protons for CO reduction by nitrogenase is water, not hydrogen gas (16).

The second line of evidence demonstrating that the hydrogen concentration does not influence nitrogenase methane isotope fractionation is based on comparing the fractionations observed in different growth containers and for the different strains. For a given growth container and strain, cell density and hydrogen concentration are correlated (Fig. 6A; also see S.I. Discussion). However, their respective effects on fractionation can be disentangled by comparing data from the Balch tubes (10 mL medium : 17 mL headspace) and serum vials (180 mL medium : 60 mL headspace). As seen in Figure 6, hydrogen and carbon isotope fractionations in cultures with 10 to 20% H_2 in their headspace at harvest overlap with those of cultures with 20 to 50% H_2 in their headspace at harvest ($p > 0.5$; Figs. 6C, E). We conclude that fractionation during methane production by nitrogenase is not sensitive to hydrogen concentration over the large range (10 to 50%) tested here. This is compatible with findings that CO_2 reduction by Mo-nitrogenase is not competitively inhibited by H_2 and does not proceed through the same reversible *re* (reductive elimination of H_2) step as N_2 reduction (64). The lack of hydrogen partial pressure dependency on fractionation contrasts with some modes of *mcr*-based methanogenesis.

Mechanistic implications for nitrogenase

Determining whether isotope effects are due to equilibrium or kinetic fractionation and under what conditions they are fully expressed can help elucidate the mechanism, intermediates, and reversibility of a reaction. At 20°C, the equilibrium hydrogen isotope fractionation predicted between methane and water is only $^{2}\alpha_{H2O/CH4} \sim 1.019$ (65). This is much smaller than the fractionation observed for nitrogenase, suggesting that kinetic, rather than equilibrium, isotope effects are responsible for the large hydrogen isotope fractionation observed here. This conclusion is consistent with the finding that fractionation of CO_2 reduction by nitrogenase is

larger at colder temperatures (Fig. 5B, F), which is generally incompatible with an equilibrium isotope effect (66). These results lead us to attribute the fractionation observed here to a kinetic isotope effect (KIE) in which CH_4 methane production by V- and Fe-only nitrogenase is roughly twice as fast as CH_3D methane production ($1.820 \leq {}^{2}\alpha_{H2O/CH4} = KIE \leq 2.199$). We suggest this new value can help yield insight into the mechanism of CO_2 reduction by nitrogenase.

The mechanism of CO_2 reduction by nitrogenase is a subject of much study because of its potential industrial application as a renewable fuel source (65, 67, 68 and references therein). The observation that the hydrogen KIE during methane production is ~2 represents a new experimental constraint for these studies. Previously, the KIE for H_2 production in the absence of N_2 (i.e. E4 to E2 state, where E2 is an intermediate state in the sequential reduction of the active site to prepare for N_2 binding at E4) by the Mo-nitrogenase was used as a tool to determine the mechanism of H_2 loss during activation of the cofactor, a catalytically inefficient reaction that competes with N_2 reduction (69). Khadka and colleagues (69) demonstrated, experimentally and computationally, that the KIE of ~2.7 is due to preference for ^{1}H during protonation of the bridging Fe-hydrides by highly acidic, protonated cofactor thiols. The KIE of ~2 observed here is lower than the KIE measured for H_2 production. This hints that (1) the preference for ^{1}H might be somewhat lower for V- and Fe-only nitrogenase compared to the Mo-nitrogenase (e.g., (70–72) and references therein for examples of the effect that the cofactor and amino acid environment have on protonation and substrate selectivity). Another possibility (2) is that, because the mechanism of CO_2 reduction by nitrogenase likely involves the migratory insertion of cofactor bound CO_2 into the Fe-hydride bond (64), the preference for ^{1}H is lower for the bridging Fe-hydrides, which do not exchange with solvent at the timescales relevant to the

255 reaction, compared to protonated thiols, which do (69). It is also possible that proton tunneling,
256 which is generally thought to have a very large kinetic isotope effect (but also see 73, 74) and
257 has been proposed to occur in nitrogenase (75) could be contributing to the observed KIE,
258 though we note that the temperature effect observed here is opposite of the predicted effect for
259 tunneling (76, 77). Computational models can distinguish the rates of hydrogenation based on ^{1}H
260 and ^{2}H and might be able to shed light on whether currently proposed, multi-step mechanisms of
261 hydrogenation by nitrogenase (78–81) are compatible with the measured KIE of ~2. The
262 clumped isotopic composition of methane produced by nitrogenase could also provide additional
263 constraints.
264
265 **Environmental Relevance**
266 The carbon and hydrogen isotopes of methane are critical constraints for the attribution of
267 emissions of this potent greenhouse gas to its sources (82). Our characterization of nitrogenase's
268 biosignature helps refine the space of possible source $\delta^{13}C$ and $\delta^{2}H$ values. The characteristic
269 $\delta^{2}H$ signature of alternative nitrogenases distinguishes them from other microbial and
270 thermogenic methane sources (Fig. 2). At −550‰, the $\delta^{2}H$ of nitrogenase-derived methane falls
271 well below the lowest values, around −400‰, that have been observed for other biotic and
272 abiotic processes (2, 38).
273
274 Given the ubiquity of CO_2 in cells and in the environment, it is likely that some CH_4 production
275 is occurring whenever V- and Fe-nitrogenase are active. To determine the extent to which stable
276 isotopes can attribute methane production to alternative nitrogenase activity in environments
277 with multiple sources, we developed a simple isotopic mixing model (Fig. 7). The model

calculates the net $^{2}\alpha_{H2O/CH4}$ and $\delta^{2}H$ of the mixed methane pool given the local water isotopic composition and the relative rates of methane production from traditional methanogenesis pathways and nitrogenase activity, assuming that all hydrogen for acetoclastic methanogenesis ultimately derive from environmental water. Hydrogen isotopic compositions as low as $\delta^{2}H_{CH4}$ ~ −400‰ have been attributed to the canonical hydrogenotrophic and acetoclastic methanogenesis pathways in natural samples (2, 38). Using this value as an upper bound, we suggest that measured $^{2}\alpha_{H2O/CH4} \geq 1.65$ (shown in red in Fig. 7A) would provide evidence for alternative nitrogenase activity in natural samples. Thus, the isotopic mixing model demonstrates that methane stable isotopes can identify alternative nitrogenase activity as long as the rate of methane production from nitrogenase is faster or in the same range as anaerobic, *mcr*-based methanogenesis rates (nitrogenase methane : total methane > 0.5) and that the isotopic composition of source water must be taken into account when interpreting the relative contributions of different biotic methanogenesis pathways. The model provides quantitative bounds on the use of characteristically low $\delta^{2}H$ of methane produced by nitrogenase as a biosignature of alternative nitrogen fixation.

It is clear that methane production by the V- and Fe-only nitrogenases does not contribute quantitatively to methane production at the global scale (10). For instance, assuming generously that ~20% of the ~145 Tg annual terrestrial biological nitrogen fixation flux (~120 Tg year^{-1} from (83) corrected for underestimation by the acetylene reduction assay as described in (26)) is fixed by Fe-only nitrogenase, and recognizing that methane itself is a minor byproduct of dinitrogen reduction (~ 5×10^{-4} CH_4 : 1 N_2 for Fe-only nitrogenase, data not shown), the resultant ~0.01 Tg year^{-1} is negligible compared to total methane emissions of ~560 Tg year^{-1}

(84). Nonetheless, we hypothesize that it could influence the methane isotopic composition, and act as a biomarker for alternative nitrogenase activity, in nitrogen-limited environments with low methanogenesis rates and high alternative nitrogenase activity. The controls on alternative nitrogenase activity are not fully understood (e.g. Glazer *et al.*, 2015; Zhang *et al.*, 2016), although new tools (26, 33) are rapidly advancing our understanding of their distribution. It is now well established that alternative nitrogenases are favored under conditions of low Mo availability (27, 86), though their activity has been observed in some sedimentary environments that appeared to be Mo-replete as well (25, 26). Aerobic soils, cyanolichens, mosses and other biocrusts, lake and marine waters (8, 87), or sediment systems with high sulfate concentrations, where sulfate reducers generally outcompete methanogens for substrates (3, 88), are possible targets to test when alternative nitrogenases are active using methane stable isotopes (10). We note that, in the global inventory of methane isotopic data, the single lowest δ^2H composition of −442‰ was recorded during the fall in northern Canada (38, 89), which coincides seasonally and spatially with measurements of high alternative nitrogenase activity in boreal cyanolichens (27, 28). This presents an exciting avenue for future research aimed at constraining the importance of nitrogenase to methane production in environments with low activity of canonical methanogens, and at illuminating the mechanism(s) of nitrogenase CO_2 reduction.

Conclusion

The alternative V- and Fe-only nitrogenases are important enzymes in the global nitrogen cycle. The curious observation that these enzymes produce methane as a minor byproduct of nitrogen fixation led us investigate how its isotopic compostion compares to other natural methane sources. Here we show that the natural abundance deuterium to hydrogen ratio of methane

derived from nitrogenase is significantly lower than methane from all other known processes, with δ^2H as low as −550‰. This result provides new experimental constraints on the mechanism of the nitrogenase enzyme and demonstrates that significantly depleted hydrogen stable isotopic composition constitute a passive biosignature of V- and Fe-only nitrogenase-derived methane. This isotopic fingerprint offers a means to probe the contribution of alternative nitrogen fixation and nitrogenase methane emissions on Earth and beyond.

Materials Methods

Bacterial cultures. *Rhodopseudomonas palustris* strains CGA766 ("V-nitrogenase strain," genotype: Δ*nifH nifD::Tn5* Δ*anfA*) and CGA755 ("Fe-only nitrogenase strain," genotype: Δ*nifH* Δ*vnfH*) were grown in batch cultures at 14, 19 and 30°C and ~90 μmols photons m^{-2} s^{-1} under anaerobic photoheterotrophic conditions in defined nitrogen-fixing medium with 2.5 μM Fe, 100 nM Mo, 10 μM V, Wolfe's vitamin solution, 0.0005% yeast extract and either 10 mM succinate or 20 mM acetate (33, 40, 41). Where applicable, the δ^2H of the growth medium was manipulated by adding 99.9% purity D_2O (Cambridge Isotope Laboratories, Inc.) to the growth medium. Bacterial growth was monitored by optical density (OD_{660}) using a Genesys 20 visible spectrophotometer (Thermo Fisher Scientific) and converted to cell density using the empirically observed relationship cells $mL^{-1} = 2.29 \times 10^9 \times OD_{660}$.

Analytical. Methane concentrations in the culture headspaces were measured either on a Peak Performer 1 gas chromatograph with N_2 carrier gas (Peak Laboratories) or on a GC-8A with He carrier gas (Shimadzu Instruments; column = Supelco HayeSep N; column temperature = 80°C; detector temperature = 150°C) with flame ionization detectors. Calibration curves were made by sequentially diluting 100 ppm or 1% CH_4 standards with N_2 in a 10 mL syringe with a luer-lock and, like the samples, loading 1 mL onto the instrument using an injection loop. Hydrogen and carbon dioxide gas concentrations were measured using gas chromatography with a thermal conductivity detector (GC-8AIT TCD, Shimadzu Instruments; column = Restek ShinCarbon ST; column temperature = 100°C; detector temperature = 150°C) with N_2 as the carrier gas. Dissolved methane was not quantified. We note that not all variables were measured in all

samples, and that the raw datapoints used for all the figures and calculations in this manuscript are available in the S.I.

Stable Isotope Measurements. Methane samples were analyzed for δ^2H and $\delta^{13}C$ at the UC Davis Stable Isotope Facility. Depending on the methane concentration, samples were collected either in pre-evacuated 12 mL soda glass vials (Labco Limited; 839W) or diluted in He-flushed vials. Because sample methane δ^2H was depleted relative to the lowest standard available at the UC Davis Stable Isotope Facility (−276‰), a dilution series of a single sample was measured, and the resulting linearity correction applied to all samples (calculations included in the S.I. Table). The constant hydrogen isotope fractionation observed for Fe-only nitrogenase over a >500‰ range in δ^2H suggests that the analytical methods employed are robust (Fig. 3). Samples for $\delta^{13}C$ analysis of CO_2 were collected in the same manner as those for methane. Samples for $\delta^{13}C$ of DIC were collected in He-flushed vials that contained 1 mL of concentrated HPLC grade phosphoric acid (85%; Fisher Chemical). At the UC Davis Stable Isotope Facility, the δ^2H_{CH4}, $\delta^{13}C_{CH4}$, $\delta^{13}C_{CO2}$ and $\delta^{13}C_{DIC}$ samples were measured on a Delta V Plus IRMS (Thermo Scientific, Bremen, Germany) coupled to a Gas Bench II system. Water δ^2H samples were collected by filtering growth medium (0.22μm) at the end of the experiment and storing at −20°C. For analysis, samples were thawed and 1.4 - 1.5 mL were aliquoted into 2 mL soda glass vials (Thermo Scientific, National C4010-1W with C4010-40A caps) and shipped on ice or at room temperature overnight to the UC Davis Stable Isotope Facility, where they were measured on a Laser Water Isotope Analyzer V2 (Los Gatos Research, Inc.). Biomass and substrate $\delta^{13}C$ were measured in the Zhang stable isotope laboratory at Princeton as described previously (41) on a Vario ISOTOPE select (Elementar Isoprime). The standard deviation of standard material

375 replicates were < 1‰ for δ^2H_{H2O}, < 2‰ for δ^2H_{CH4}, < 0.2‰ for $\delta^{13}C_{CH4}$ (> 10 ppm), < 0.2‰
376 for $\delta^{13}C_{CO2}$ and $\delta^{13}C_{DIC}$, and < 0.1‰ for $\delta^{13}C_{biomass}$.
377
378 ***Isotope Calculations***. Hydrogen and carbon isotopes are expressed using delta notation relative
379 to Vienna Standard Mean Ocean Water (VSMOW) and Vienna Pee Dee Belemnite (VPDB),
380 respectively. Apparent CO_2-CH_4 and water-CH_4 isotope fractionation factors were calculated as
381 substrate over product using the equations:
382 $^{13}\alpha_{CO2/CH4} = {}^{13}R_{CO2}/{}^{13}R_{CH4} = (\delta^{13}C_{CO2}+1000)/(\delta^{13}C_{CH4}+1000)$
383 $^{2}\alpha_{H2O/CH4} = {}^{2}R_{H2O}/{}^{2}R_{CH4} = (\delta^{2}H_{H2O}+1000)/(\delta^{2}H_{CH4}+1000)$
384 $\varepsilon = (\alpha-1)*1000‰$
385 In this manuscript, errors represent the standard error of multiple biological replicates.
386
387 ***Isotope Mixing Model.*** To determine under what conditions the methane isotopic composition
388 can be used as a biosignature for alternative nitrogenase activity, we developed a mixing model
389 that calculates the fractionation and isotopic composition of methane produced by multiple
390 sources (Fig. 7). We used the following parameters: $^{2}\alpha_{Nase} = 2.07$; $\delta^2H_{H2O} = -40‰$ vs. VSMOW
391 as representative of the mid-latitudes and −150‰ vs. SVMOW as representative of northern
392 latitudes; and k = methane produced by nitrogenase : total methane produced by nitrogenase and
393 *mcr*-based anaerobic methanogenesis. For fermentative methanogenesis, the model assumes that
394 all protons ultimately derive from local water. The observed fractionation and isotopic
395 composition were calculated using the equations:
396 $^{2}F_{Nase/mcrCH4} = {}^{2}R_{Nase/mcrCH4}/(1+{}^{2}R_{Nase/mcrCH4})$
397 $^{2}F_{CH4} = k*{}^{2}F_{NaseCH4} + (1-k)*{}^{2}F_{mcrCH4}$

***Data Availability*.** Individual datapoints are available in the S.I. Table. In addition to the S.I. Table, these data will be uploaded in FigShare prior to publication.

Acknowledgements

We thank Richard Doucett and Elvira Delgado of the UC Davis Stable Isotope Facility for the isotopic analysis of the water, methane, CO_2 and DIC samples in this project, and Lina Taenzer, Rachel Harris and Barbara Sherwood Lollar for useful discussions. Ashley Maloney and Emma Bertran provided valuable feedback on drafts of this paper. Funding for this project was provided by the National Science Foundation and National Aeronautics and Space Administration (NSF Award# EAR1631814 and NASA Award# 80NSSC17K0667 to XZ), an NSF Graduate Research Fellowship to KEL, the Princeton Environmental Institute through the Walbridge Fund, the Simons Foundation division of Life Sciences (XZ, WDL), and the Dartmouth College Vice-Provost for Research (WDL).

References

1. Dean JF, Middelburg JJ, Röckmann T, Aerts R, Blauw LG, Egger M, Jetten MSM, de Jong AEE, Meisel OH, Rasigraf O, Slomp CP, in't Zandt MH, Dolman AJ. 2018. Methane Feedbacks to the Global Climate System in a Warmer World. Rev Geophys 56:207–250.
2. Whiticar MJ. 1999. Carbon and hydrogen isotope systematics of bacterial formation and oxidation of methane. Chem Geol 161:291–314.
3. Schönheit P, Keweloh H, Thauer RK. 1981. Factor F420 degradation in *Methanobacterium thermoautotrophicum* during exposure to oxygen. FEMS Microbiol Lett 12:347–349.
4. Schlesinger WH, Bernhardt ES. 2013. Chapter 7 - Wetland Ecosystems, p. 233–274. *In* Schlesinger, WH, Bernhardt, ESBT-B (Third E (eds.), . Academic Press, Boston.
5. Fenchel T, King GM, Blackburn TH. 2012. Chapter 1 - Bacterial Metabolism, p. 1–34. *In* Fenchel, T, King, GM, Blackburn, THBT-BB (Third E (eds.), . Academic Press, Boston.
6. Metcalf WW, Griffin BM, Cicchillo RM, Gao J, Janga SC, Cooke HA, Circello BT, Evans BS, Martens-Habbena W, Stahl DA, van der Donk WA. 2012. Synthesis of Methylphosphonic Acid by Marine Microbes: A Source for Methane in the Aerobic Ocean. Science (80-) 337:1104 LP – 1107.
7. Repeta DJ, Ferrón S, Sosa OA, Johnson CG, Repeta LD, Acker M, DeLong EF, Karl DM. 2016. Marine methane paradox explained by bacterial degradation of dissolved organic matter. Nat Geosci 9:884.
8. Taenzer L, Carini PC, Masterson AM, Bourque B, Gaube JH, Leavitt WD. 2020. Microbial Methane from Methylphosphonate Isotopically Records Source. Geophys Res Lett e60053.
9. Schauder R, Eikmanns B, Thauer RK, Widdel F, Fuchs G. 1986. Acetate oxidation to CO_2 in anaerobic bacteria via a novel pathway not involving reactions of the citric acid cycle. Arch Microbiol 145:162–172.
10. Zheng Y, Harris DF, Yu Z, Fu Y, Poudel S, Ledbetter RN, Fixen KR, Yang Z-Y, Boyd ES, Lidstrom ME, Seefeldt LC, Harwood CS. 2018. A pathway for biological methane production using bacterial iron-only nitrogenase. Nat Microbiol 3:281–286.
11. Fowler D, Coyle M, Skiba U, Sutton MA, Cape JN, Reis S, Sheppard LJ, Jenkins A, Grizzetti B, Galloway JN, Vitousek P, Leach A, Bouwman AF, Butterbach-Bahl K, Dentener F, Stevenson D, Amann M, Voss M. 2013. The global nitrogen cycle in the twenty-first century. Philos Trans R Soc B Biol Sci 368:20130164.
12. Vitousek PM, Menge DNL, Reed SC, Cleveland CC. 2013. Biological nitrogen fixation: rates, patterns and ecological controls in terrestrial ecosystems. Philos Trans R Soc B Biol Sci 368:20130119.
13. Seefeldt LC, Yang Z-Y, Duval S, Dean DR. 2013. Nitrogenase reduction of carbon-containing compounds. Biochim Biophys Acta - Bioenerg 1827:1102–1111.
14. Lee CC, Fay AW, Weng T-C, Krest CM, Hedman B, Hodgson KO, Hu Y, Ribbe MW. 2015. Uncoupling binding of substrate CO from turnover by vanadium nitrogenase. Proc Natl Acad Sci 112:13845 LP – 13849.
15. Lee CC, Hu Y, Ribbe MW. 2010. Vanadium Nitrogenase Reduces CO. Science 329:642.
16. Hu Y, Lee CC, Ribbe MW. 2011. Extending the Carbon Chain: Hydrocarbon Formation Catalyzed by Vanadium/Molybdenum Nitrogenases. Science 333:753.

17. Yang Z-Y, Dean DR, Seefeldt LC. 2011. Molybdenum nitrogenase catalyzes the reduction and coupling of CO to form hydrocarbons. J Biol Chem 286:19417–19421.
18. Chisnell JR, Premakumar R, Bishop PE. 1988. Purification of a second alternative nitrogenase from a nifHDK deletion strain of Azotobacter vinelandii. J Bacteriol 170:27–33.
19. Hales BJ, Case EE, Morningstar JE, Dzeda MF, Mauterer LA. 1986. Isolation of a new vanadium-containing nitrogenase from Azotobacter vinelandii. Biochemistry 25:7251–7255.
20. Dilworth MJ. 1966. Acetylene reduction by nitrogen-fixing preparations from Clostridium pasteurianum. Biochim Biophys Acta 127:285–294.
21. Schollhorn R, Burris R. 1966. Study of intermediates in nitrogen fixation. Fed Proc 25:710.
22. Bellenger JP, Xu Y, Zhang X, Morel FMM, Kraepiel AML. 2014. Possible contribution of alternative nitrogenases to nitrogen fixation by asymbiotic N_2-fixing bacteria in soils. Soil Biol Biochem 69:413–420.
23. Stewart WD, Fitzgerald GP, Burris RH. 1967. In situ studies on N_2 fixation using the acetylene reduction technique. Proc Natl Acad Sci 58:2071–2078.
24. Hardy RW, Holsten RD, Jackson EK, Burns RC. 1968. The acetylene-ethylene assay for N_2 fixation: laboratory and field evaluation. Plant Physiol 43:1185–1207.
25. McRose DL, Zhang X, Kraepiel AML, Morel FMM. 2017. Diversity and Activity of Alternative Nitrogenases in Sequenced Genomes and Coastal Environments. Front Microbiol
26. Zhang X, McRose DL, Darnajoux R, Bellenger JP, Morel FMM, Kraepiel AML. 2016. Alternative nitrogenase activity in the environment and nitrogen cycle implications. Biogeochemistry 127:189–198.
27. Darnajoux R, Magain N, Renaudin M, Lutzoni F, Bellenger J-P, Zhang X. 2019. Molybdenum threshold for ecosystem scale alternative vanadium nitrogenase activity in boreal forests. Proc Natl Acad Sci 116:24682.
28. Darnajoux R, Zhang X, McRose DL, Miadlikowska J, Lutzoni F, Kraepiel AML, Bellenger J-P. 2017. Biological nitrogen fixation by alternative nitrogenases in boreal cyanolichens: importance of molybdenum availability and implications for current biological nitrogen fixation estimates. New Phytol 213:680–689.
29. Hodkinson BP, Allen JL, Forrest LL, Goffinet B, Sérusiaux E, Andrésson ÓS, Miao V, Bellenger J-P, Lutzoni F. 2014. Lichen-symbiotic cyanobacteria associated with Peltigera have an alternative vanadium-dependent nitrogen fixation system. Eur J Phycol 49:11–19.
30. Betancourt DA, Loveless TM, Brown JW, Bishop PE. 2008. Characterization of Diazotrophs Containing Mo-Independent Nitrogenases, Isolated from Diverse Natural Environments. Appl Environ Microbiol 74:3471.
31. Yang Z-Y, Moure VR, Dean DR, Seefeldt LC. 2012. Carbon dioxide reduction to methane and coupling with acetylene to form propylene catalyzed by remodeled nitrogenase. Proc Natl Acad Sci 109:19644.
32. Fixen KR, Zheng Y, Harris DF, Shaw S, Yang Z-Y, Dean DR, Seefeldt LC, Harwood CS. 2016. Light-driven carbon dioxide reduction to methane by nitrogenase in a photosynthetic bacterium. Proc Natl Acad Sci 113:10163.
33. Zhang X, Sigman DM, Morel FMM, Kraepiel AML. 2014. Nitrogen isotope fractionation by alternative nitrogenases and past ocean anoxia. Proc Natl Acad Sci 111:4782–4787.

34. Whiticar MJ, Faber E, Schoell M. 1986. Biogenic methane formation in marine and freshwater environments: CO_2 reduction vs. acetate fermentation—Isotope evidence. Geochim Cosmochim Acta 50:693–709.
35. Schoell M. 1980. The hydrogen and carbon isotopic composition of methane from natural gases of various origins. Geochim Cosmochim Acta 44:649–661.
36. Etiope G, Sherwood Lollar B. 2013. Abiotic methane on earth. Rev Geophys 51:276–299.
37. Penger J, Conrad R, Blaser M. 2012. Stable carbon isotope fractionation by methylotrophic methanogenic archaea. Appl Environ Microbiol 78:7596–7602.
38. Sherwood OA, Schwietzke S, Arling VA, Etiope G. 2017. Global Inventory of Gas Geochemistry Data from Fossil Fuel, Microbial and Burning Sources, version 2017. Earth Syst Sci Data 9:639–656.
39. Conrad R. 2005. Quantification of methanogenic pathways using stable carbon isotopic signatures: a review and a proposal. Org Geochem 36:739–752.
40. Oda Y, Wu L, Liu X, Yan T, Zhou J, Harwood CS, Samanta SK, Rey FE, Wu L, Liu X, Yan T, Zhou J, Harwood CS, Samanta SK, Rey FE, Rey, Wu L, Liu X, Yan T, Zhou J, Harwood CS, Rey FE. 2005. Functional Genomic Analysis of Three Nitrogenase Isozymes in the Photosynthetic Bacterium Rhodopseudomonas palustris. J Bacteriol 187:7784–7794.
41. Luxem KE, Kraepiel AML, Zhang L, Waldbauer JR, Zhang X. 2020. Carbon substrate re-orders relative growth of a bacterium using Mo-, V-, or Fe-nitrogenase for nitrogen fixation. Environ Microbiol 22:1397-1408.
42. Valentine DL, Chidthaisong A, Rice A, Reeburgh WS, Tyler SC. 2004. Carbon and hydrogen isotope fractionation by moderately thermophilic methanogens. Geochim Cosmochim Acta 68:1571–1590.
43. Tazaz AM, Bebout BM, Kelley CA, Poole J, Chanton JP. 2013. Redefining the isotopic boundaries of biogenic methane: Methane from endoevaporites. Icarus 224:268–275.
44. Zheng Y, Harwood CS. 2019. Influence of Energy and Electron Availability on In Vivo Methane and Hydrogen Production by a Variant Molybdenum Nitrogenase. Appl Environ Microbiol 85:e02671-18.
45. House CH, Schopf JW, Stetter KO. 2003. Carbon isotopic fractionation by Archaeans and other thermophilic prokaryotes. Org Geochem 34:345–356.
46. McKinlay JB, Harwood CS. 2010. Carbon dioxide fixation as a central redox cofactor recycling mechanism in bacteria. Proc Natl Acad Sci 107:11669–11675.
47. McKinlay JB, Harwood CS. 2011. Calvin Cycle Flux , Pathway Constraints, and Substrate Oxidation State. MBio 2:1–9.
48. Simpson FB, Burris RH. 1984. A nitrogen pressure of 50 atmospheres does not prevent evolution of hydrogen by nitrogenase. Science 224:1095–1097.
49. Harris DF, Lukoyanov DA, Kallas H, Trncik C, Yang Z-Y, Compton P, Kelleher N, Einsle O, Dean DR, Hoffman BM, Seefeldt LC. 2019. Mo-, V-, and Fe-Nitrogenases Use a Universal Eight-Electron Reductive-Elimination Mechanism To Achieve N_2 Reduction. Biochemistry.
50. Penning H, Plugge CM, Galand PE, Conrad R. 2005. Variation of carbon isotope fractionation in hydrogenotrophic methanogenic microbial cultures and environmental samples at different energy status. Glob Chang Biol 11:2103–2113.
51. Burke RA. 1993. Possible influence of hydrogen concentration on microbial methane stable hydrogen isotopic composition. Chemosphere 26:55–67.

52. Hornibrook ERC, Longstaffe FJ, Fyfe WS. 1997. Spatial distribution of microbial methane production pathways in temperate zone wetland soils: Stable carbon and hydrogen isotope evidence. Geochim Cosmochim Acta 61:745–753.
53. Sugimoto A, Wada E. 1995. Hydrogen isotopic composition of bacterial methane: CO_2/H_2 reduction and acetate fermentation. Geochim Cosmochim Acta 59:1329–1337.
54. Sugimoto A, Fujita N. 2006. Hydrogen Concentration and Stable Isotopic Composition of Methane in Bubble Gas Observed in a Natural Wetland. Biogeochemistry 81:33–44.
55. Pester M, Tholen A, Friedrich MW, Brune A. 2007. Methane oxidation in termite hindguts: absence of evidence and evidence of absence. Appl Environ Microbiol 73:2024–2028.
56. Chidthaisong A, Chin K-J, Valentine DL, Tyler SC. 2002. A comparison of isotope fractionation of carbon and hydrogen from paddy field rice roots and soil bacterial enrichments during CO_2/H_2 methanogenesis. Geochim Cosmochim Acta 66:983–995.
57. Balabane M, Galimov E, Hermann M, Létolle R. 1987. Hydrogen and carbon isotope fractionation during experimental production of bacterial methane. Org Geochem 11:115–119.
58. Topçuoğlu BD, Meydan C, Nguyen TB, Lang SQ, Holden JF. 2019. Growth Kinetics, Carbon Isotope Fractionation, and Gene Expression in the Hyperthermophile Methanocaldococcus jannaschii during Hydrogen-Limited Growth and Interspecies Hydrogen Transfer. Appl Environ Microbiol 85:e00180-19.
59. Rey FE, Oda Y, Harwood CS. 2006. Regulation of Uptake Hydrogenase and Effects of Hydrogen Utilization on Gene Expression in Rhodopseudomonas palustris. J Bacteriol 188:6143.
60. Dance I. 2013. Nitrogenase: a general hydrogenator of small molecules. Chem Commun 49:10893–10907.
61. Wang DT, Reeves EP, McDermott JM, Seewald JS, Ono S. 2018. Clumped isotopologue constraints on the origin of methane at seafloor hot springs. Geochim Cosmochim Acta 223:141–158.
62. Pester NJ, Conrad ME, Knauss KG, DePaolo DJ. 2018. Kinetics of D/H isotope fractionation between molecular hydrogen and water. Geochim Cosmochim Acta 242:191–212.
63. Sessions AL, Sylva SP, Summons RE, Hayes JM. 2004. Isotopic exchange of carbon-bound hydrogen over geologic timescales. Geochim Cosmochim Acta 68:1545–1559.
64. Khadka N, Dean DR, Smith D, Hoffman BM, Raugei S, Seefeldt LC. 2016. CO_2 Reduction Catalyzed by Nitrogenase: Pathways to Formate, Carbon Monoxide, and Methane. Inorg Chem 55:8321–8330.
65. Bottinga Y. 1969. Calculated fractionation factors for carbon and hydrogen isotope exchange in the system calcite-carbon dioxide-graphite-methane-hydrogen-water vapor. Geochim Cosmochim Acta 33:49–64.
66. Urey HC. 1947. The thermodynamic properties of isotopic substances. J Chem Soc 562–581.
67. Sickerman NS, Hu Y, Ribbe MW. 2017. Activation of CO_2 by Vanadium Nitrogenase. Chem – An Asian J 12:1985–1996.
68. Rebelein JG, Hu Y, Ribbe MW. 2015. Widening the Product Profile of Carbon Dioxide Reduction by Vanadium Nitrogenase. Chembiochem 16:1993–1996.
69. Khadka N, Milton RD, Shaw S, Lukoyanov D, Dean DR, Minteer SD, Raugei S, Hoffman

BM, Seefeldt LC. 2017. Mechanism of Nitrogenase H_2 Formation by Metal-Hydride Protonation Probed by Mediated Electrocatalysis and H/D Isotope Effects. J Am Chem Soc 139:13518–13524.

70. Newcomb MP, Lee CC, Tanifuji K, Jasniewski AJ, Liedtke J, Ribbe MW, Hu Y. 2019. A V-Nitrogenase Variant Containing a Citrate-Substituted Cofactor. ChemBioChem.

71. Raugei S, Seefeldt LC, Hoffman BM. 2018. Critical computational analysis illuminates the reductive-elimination mechanism that activates nitrogenase for N_2 reduction. Proc Natl Acad Sci 115:E10521–E10530.

72. Chen C-Y, Chen M-L, Chen H-B, Wang H, Cramer SP, Zhou Z-H. 2014. α-Hydroxy coordination of mononuclear vanadyl citrate, malate and S-citramalate with N-heterocycle ligand, implying a new protonation pathway of iron-vanadium cofactor in nitrogenase. J Inorg Biochem 141:114–120.

73. Buchachenko AL, Pliss EM. 2016. Isotope effects of hydrogen and atom tunnelling. Russ Chem Rev 85:557–564.

74. Hama T, Ueta H, Kouchi A, Watanabe N. 2015. Quantum tunneling observed without its characteristic large kinetic isotope effects. Proc Natl Acad Sci 112:7438.

75. Dance I. 2008. The chemical mechanism of nitrogenase: hydrogen tunneling and further aspects of the intramolecular mechanism for hydrogenation of η2-N2 on FeMo-co to NH3. Dalt Trans 5992–5998.

76. Zhang Z, Nelson DB, Sachs JP. 2014. Hydrogen isotope fractionation in algae: III. Theoretical interpretations. Org Geochem 75:1–7.

77. Basran J, Sutcliffe MJ, Scrutton NS. 2001. Deuterium isotope effects during carbon-hydrogen bond cleavage by trimethylamine dehydrogenase: Implications for mechanism and vibrationally assisted hydrogen tunneling in wild-type and mutant enzymes. J Biol Chem 276:24581–24587.

78. Dance I. 2019. Computational Investigations of the Chemical Mechanism of the Enzyme Nitrogenase. ChemBioChem.

79. Jasniewski AJ, Lee CC, Ribbe MW, Hu Y. 2020. Reactivity, Mechanism, and Assembly of the Alternative Nitrogenases. Chem Rev.

80. Hoffman BM, Lukoyanov D, Yang Z-Y, Dean DR, Seefeldt LC. 2014. Mechanism of Nitrogen Fixation by Nitrogenase: The Next Stage. Chem Rev 114:4041–4062.

81. Buscagan TM, Rees DC. 2019. Rethinking the Nitrogenase Mechanism: Activating the Active Site. Joule 3:2662–2678.

82. Ganesan AL, Schwietzke S, Poulter B, Arnold T, Lan X, Rigby M, Vogel FR, van der Werf GR, Janssens-Maenhout G, Boesch H, Pandey S, Manning AJ, Jackson RB, Nisbet EG, Manning MR. 2019. Advancing Scientific Understanding of the Global Methane Budget in Support of the Paris Agreement. Global Biogeochem Cycles 33:1475–1512.

83. Battye W, Aneja VP, Schlesinger WH. 2017. Is nitrogen the next carbon? Earth's Futur 5:894–904.

84. Saunois M, Bousquet P, Poulter B, Peregon A, Ciais P, Canadell JG, Dlugokencky EJ, Etiope G, Bastviken D, Houweling S, Janssens-Maenhout G, Tubiello FN, Castaldi S, Jackson RB, Alexe M, Arora VK, Beerling DJ, Bergamaschi P, Blake DR, Brailsford G, Brovkin V, Bruhwiler L, Crevoisier C, Crill P, Covey K, Curry C, Frankenberg C, Gedney N, Höglund-Isaksson L, Ishizawa M, Ito A, Joos F, Kim H-S, Kleinen T, Krummel P, Lamarque J-F, Langenfelds R, Locatelli R, Machida T, Maksyutov S, McDonald KC, Marshall J, Melton JR, Morino I, Naik V, O'Doherty S, Parmentier F-JW, Patra PK, Peng

C, Peng S, Peters GP, Pison I, Prigent C, Prinn R, Ramonet M, Riley WJ, Saito M, Santini M, Schroeder R, Simpson IJ, Spahni R, Steele P, Takizawa A, Thornton BF, Tian H, Tohjima Y, Viovy N, Voulgarakis A, van Weele M, van der Werf GR, Weiss R, Wiedinmyer C, Wilton DJ, Wiltshire A, Worthy D, Wunch D, Xu X, Yoshida Y, Zhang B, Zhang Z, Zhu Q. 2016. The global methane budget 2000–2012. Earth Syst Sci Data 8:697–751.

85. Glazer AN, Kechris K, Howard JB. 2015. Distribution and Ecological Niches of Nitrogenases. Biol Nitrogen Fixat.

86. Bellenger J-P, Wichard T, Xu Y, Kraepiel AML. 2011. Essential metals for nitrogen fixation in a free-living N2-fixing bacterium: chelation, homeostasis and high use efficiency. Environ Microbiol 13:1395–1411.

87. Khatun S, Iwata T, Kojima H, Fukui M, Aoki T, Mochizuki S, Naito A, Kobayashi A, Uzawa R. 2019. Aerobic methane production by planktonic microbes in lakes. Sci Total Environ 696:133916.

88. Achtnich C, Bak F, Conrad R. 1995. Competition for electron donors among nitrate reducers, ferric iron reducers, sulfate reducers, and methanogens in anoxic paddy soil. Biol Fertil Soils 19:65–72.

89. Kuhlmann AJ, Worthy DEJ, Trivett NBA, Levin I. 1998. Methane emissions from a wetland region within the Hudson Bay Lowland: An atmospheric approach. J Geophys Res Atmos 103:16009–16016.

90. Niemann M, Whiticar MJ. 2017. Stable Isotope Systematics of Coalbed Gas during Desorption and Production. Geosciences 7.

667 **Fig. 1. Growth dynamics and methane yields of nitrogenase strains.** During growth (**A**) on
668 succinate at 19°C**,** the *R. palustris* V- and Fe-only nitrogenase strains produced methane (**B)**. The
669 Fe-only nitrogenase strain produced >10-fold more methane in the headspace than the V-
670 nitrogenase strain. For the Fe-nitrogenase strain, methane production per cell is greater at higher
671 cell densities. Error bars show the standard error of three biological replicates. Dissolved
672 methane is not included.

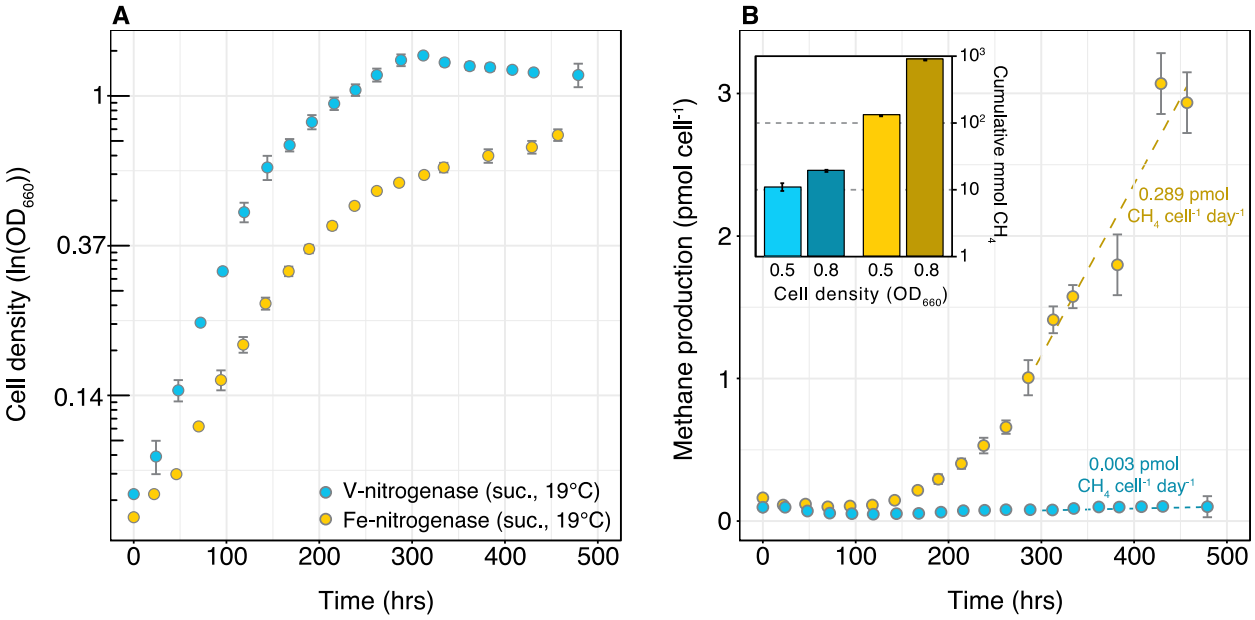

673

674

675 **Fig. 2. Nitrogenase-derived methane has a unique stable isotopic composition.** The stable
676 isotopic composition of methane produced by nitrogenase (yellow) can be distinguished from
677 other natural methane sources due to its more depleted hydrogen isotopic composition.
678 Individual datapoints from this study are shown as diamonds (◊, n = 31). The observed range for
679 fermentative (green), hydrogenotrophic (blue) and geological (red) methane sources were taken
680 from (90), though we note that these boundaries are not absolute (e.g. (36)).

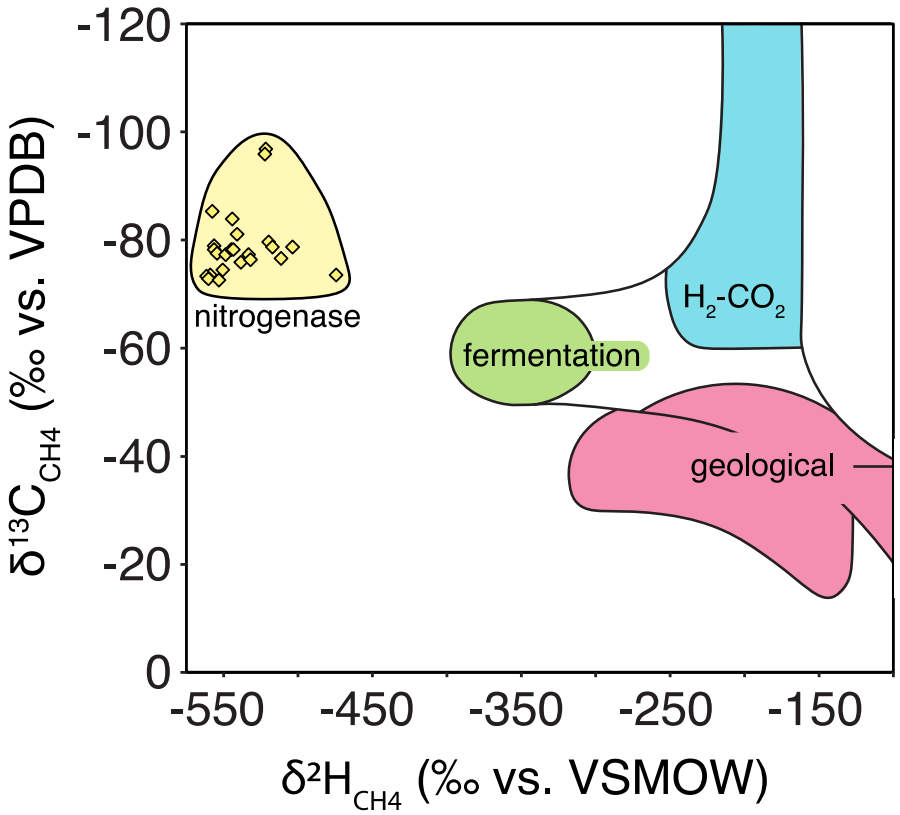

681

682

683 **Fig. 3. Hydrogen isotope fractionation does not depend on water isotopic composition.**
684 Regression of δ^2H values for source water versus methane show that hydrogen isotope
685 fractionation ($^2\alpha_{H2O/CH4}$) is constant over a 600‰ range for the Fe-only nitrogenase strain grown
686 at 19°C on succinate. The hydrogen isotope fractionation calculated using the slope ($^2\alpha_{H2O/CH4}$ =
687 2.056 ± 0.057, mean ± SE), intercept ($^2\alpha_{H2O/CH4}$ = 1050/1000 + 1 ± 19/1000 = 2.050 ± 0.019) and
688 individual samples ($^2\alpha_{H2O/CH4}$ = 2.047 ± 0.016) is indistinguishable ($p \geq 0.9$). The values next to
689 each data point are the calculated fractionations for individual samples and the shaded area
690 shows the 95% confidence interval for the regression. N.B. The convention used for individual
691 samples is for substrate over product, whereas the regression line was calculated as product over
692 substrate. The regression calculated for substrate over product, x = (2.043 ± 0.117) y + (1045 ±
693 46), is statistically indistinguishable ($p \geq 0.9$).

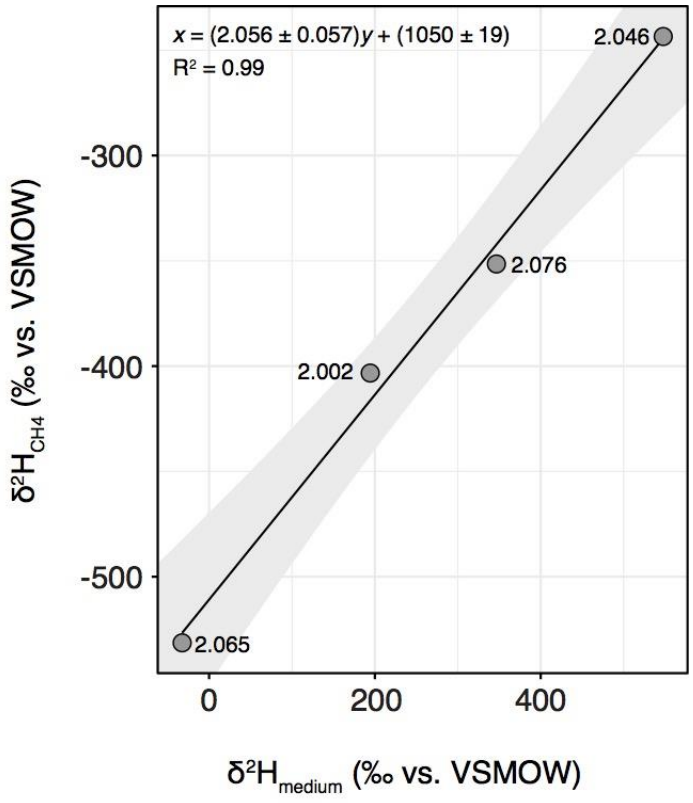

694

695

696 **Fig. 4. Nitrogenase-derived methane has a charachteristic hydrogen isotope fractionation.**
697 The largest hydrogen isotope fractionations observed for canonical, *mcr*-based anaerobic
698 methanogenesis pathways, around ~ 1.45 (34, 42), are substantially smaller than the hydrogen
699 isotope fractionation observed for nitrogenase (**A**). However, carbon isotope fractionation (**B**) by
700 nitrogenase falls within the the range observed for hydrogenotrophic methanogenesis (blue;
701 $1.023 \leq {}^{13}\alpha_{CO2/CH4} \leq 1.090$) and is intermediate to the range observed for methanol- ($1.072 \leq$
702 ${}^{13}\alpha_{CO2/CH4} \leq 1.094$) and acetate- ($1.017 \leq {}^{13}\alpha_{CO2/CH4} \leq 1.031$) based fermentative methanogenesis
703 (green; 8). Green-blue hatched areas represent ranges of overlap between the fractionation
704 obuserved for fermentative and hydrogenotrophic methanogenesis. Individual datapoints from
705 this study are shown as yellow diamonds (◊).

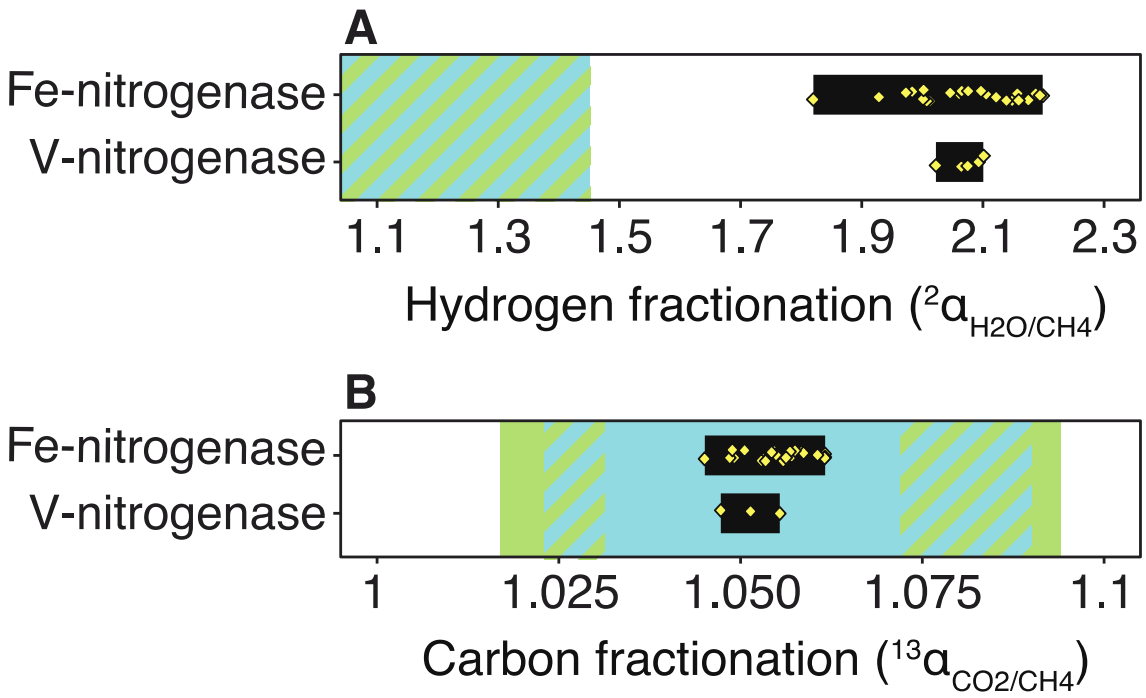

706

707

Fig. 5. Carbon and hydrogen isotope fractionations associated with methane production by nitrogenase under different growth conditions. Hydrogen and carbon isotope fractionations increase at low temperatures (**B**, **F**), higher cell densities (**C**, **G**) and higher substrate concentrations (**D**, **H**). Hydrogen isotope fractionation is comparable during growth on different organic carbon substrates (succinate, suc.; acetate, ac.) and when the growth medium is acidified (suc.‡; **A**). Carbon isotope fractionation is slightly higher during growth on acetate than on succinate (**E**) although this could also be related to differences in the cell density at harvest (**G**). The dissolved inorganic carbon (DIC) concentration (**I**) and inorganic carbon isotopic composition (**J**) increase throughout exponential growth, suggesting that substrate concentration could be influencing the observed effect of cell density (OD_{660}) on fractionation. The boxplots in panels **A**, **B**, **E** and **F** show the median (center line), first and third quartiles (outer lines), and values within 1.5 times the inner quartile range (whiskers). For panel **J**, note that, for some samples, only $\delta^{13}C_{CO2}$ or $\delta^{13}C_{DIC}$ were measured, such that $^{13}C_{CO2}$ or $\delta^{13}C_{DIC}$ datapoints are not necessarily paired.

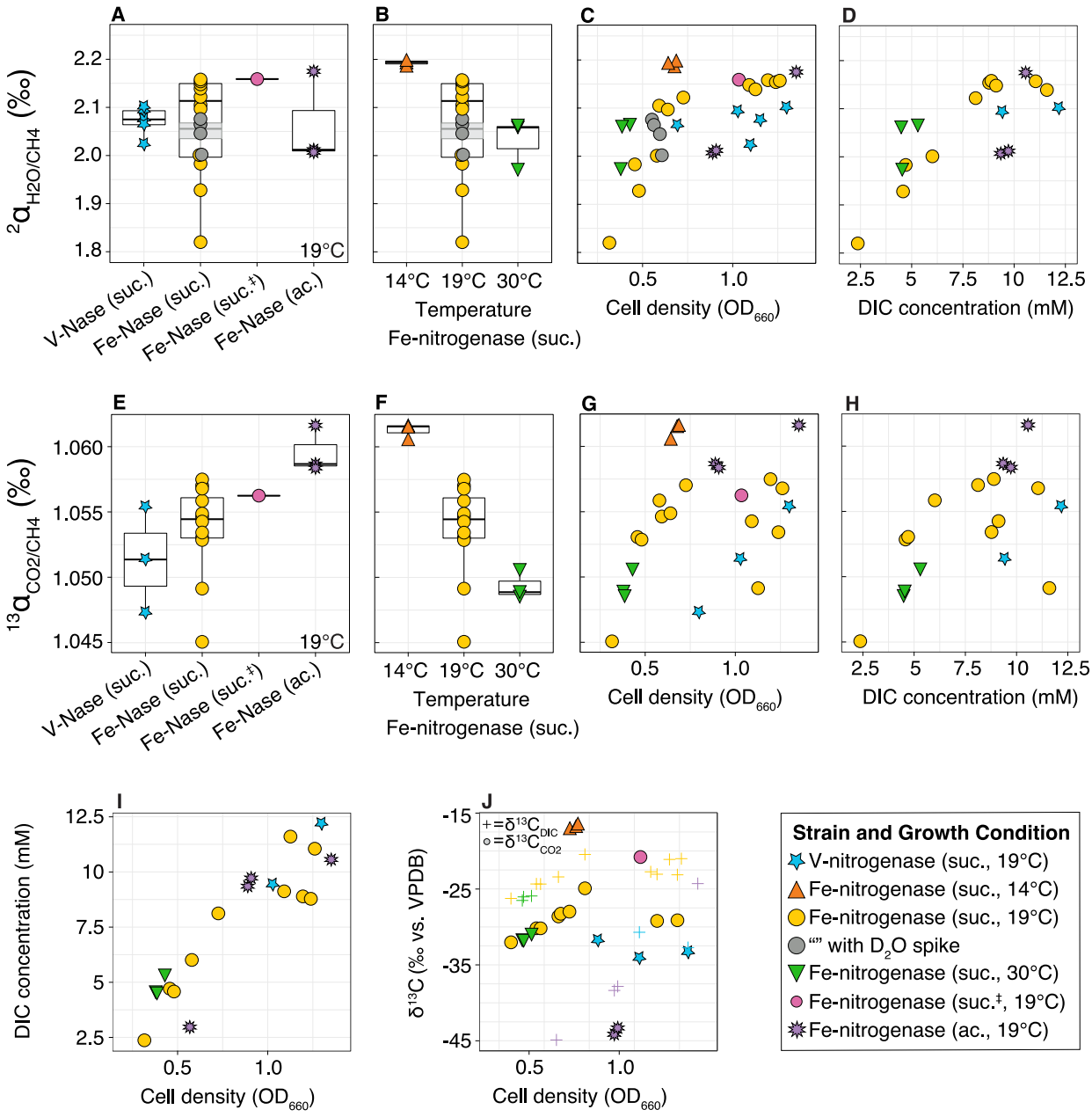

722

723 **Fig. 6. Hydrogen concentration does not alter the isotopic composition of nitrogenase**
724 **derived methane.** Strains produce hydrogen (H_2) proportional to growth. Correspondingly, the
725 cultures grown in balch tubes, which had higher headspace to volume ratios, accumulated lower
726 concentrations of hydrogen (**A**). Comparison of hydrogen (**B**) and carbon (**D**) isotope
727 fractionations between cultures grown in balch tubes and serum vials shows that hydrogen
728 concentration is not responsible for the variability in fractionation between samples: the methane
729 from cultures harvested at high cell densities in serum vials had a similar range in isotope
730 fractionation as the methane from cultures grown in balch tubes despite >2-fold differences in
731 headspace hydrogen concentrations. This is also apparent in histograms **C** and **E** which show
732 that the distribution of isotope fractionation is the same ($p > 0.5$) for cultures whose headspace
733 hydrogen concentration at harvest was between 10 and 20% (green) or 20 and 50% H_2 (blue).

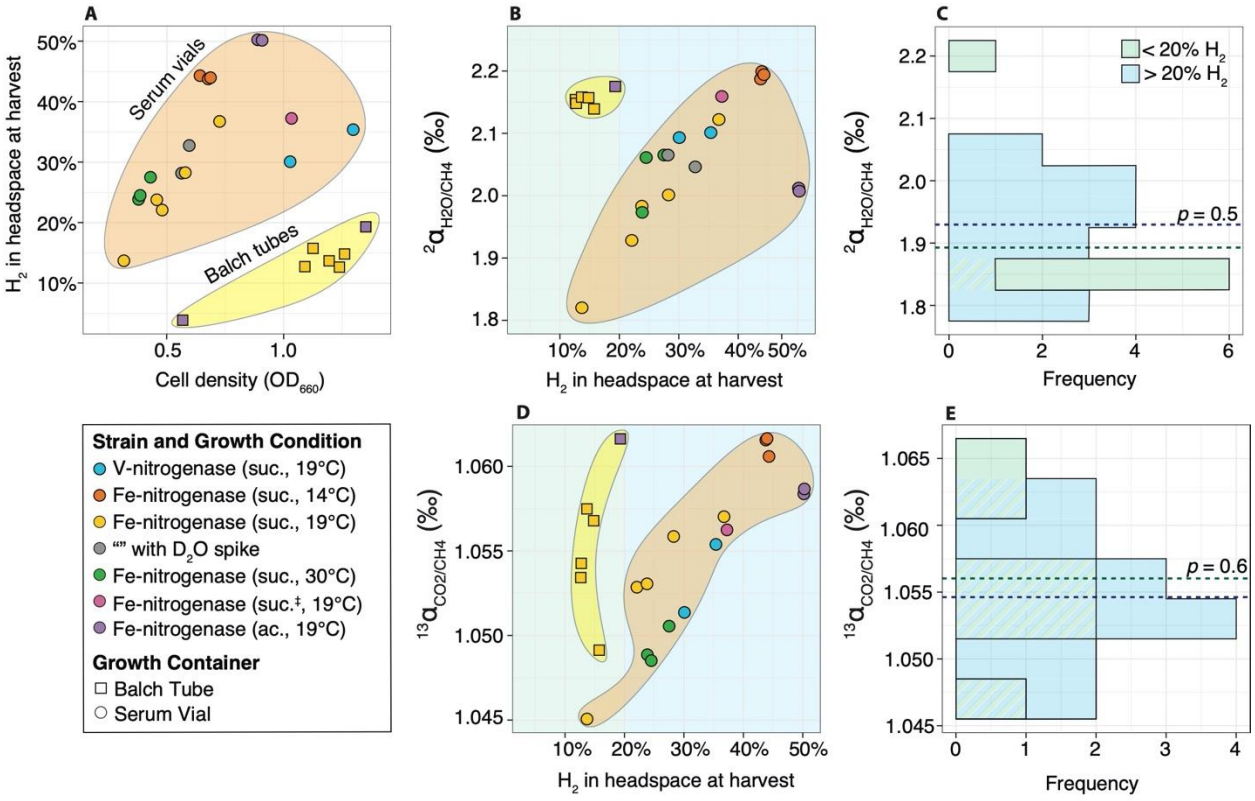

734

Fig. 7. Observed fractionation (A) and methane isotopic composition (B) for multiple methane sources. Panel A shows the apparent fractionation ($^2\alpha_{H2O/CH4}$) between water and methane in an environment with co-occurring production from nitrogenase ($^2\alpha_{H2O/CH4}$ = 2.07; x-axis shows the relative contribution of nitrogenase to the total methane pool) and a second source with $^2\alpha_{H2O/CH4}$ = 1.0 (dashed line; no expressed fractionation), $^2\alpha_{H2O/CH4}$ = 1.3 (broadly representative of hydrogenotrophic methanogenesis (34)) or $^2\alpha_{H2O/CH4}$ = 1.45 (broadly representative of acetoclastic methanogenesis (34), though values this high have also been observed for hydrogenotrophic methanogenesis (42)). Panel B shows the calculated methane isotopic composition δ^2H_{CH4} given the isotopic composition of local source water (x-axis) and the measured fractionation between water and methane ($^2\alpha_{H2O/CH4}$; y-axis). For example, for a sample with $^2\alpha_{obs}$ = 1.8 (e.g. when δ^2H_{H2O} = −100‰, δ^2H_{CH4} = −500‰, shown as a blue circle in panel B) the model predicts that ≥ 70% of the methane is produced by nitrogenase, depending on whether the competing source of methane is fermentative (blue line 1, ~70%) or hydrogenotrophic (blue line 2, ~75%).

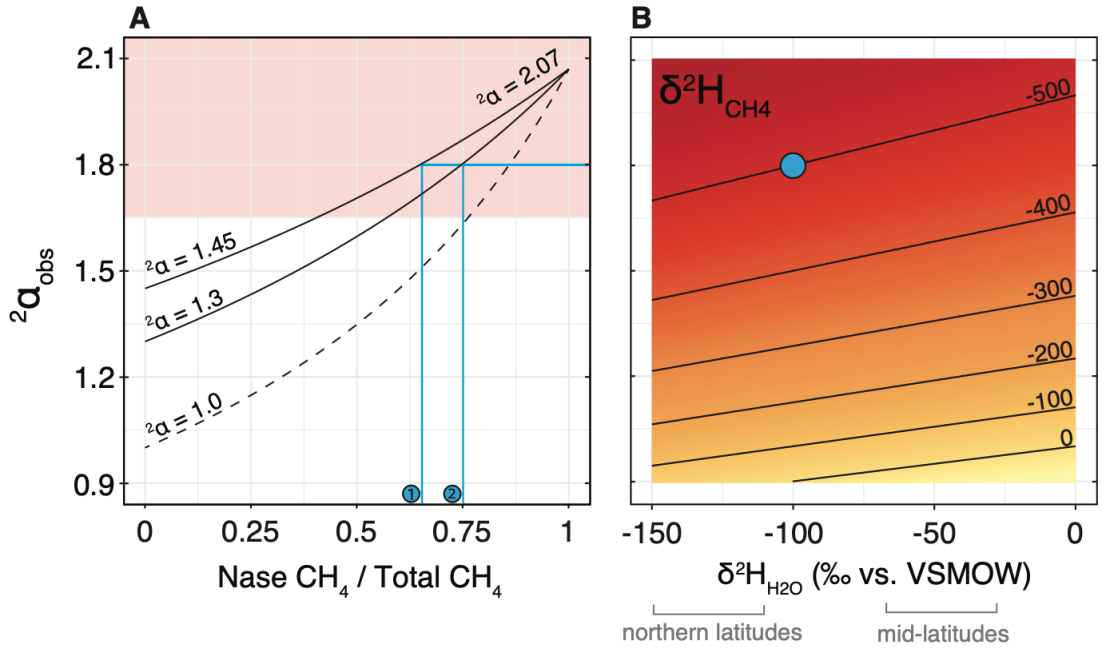

Table 1. Carbon and hydrogen stable isotope fractionation associated with methane production by V- and Fe-only nitrogenase. Compared to other methane producing pathways, the range of fractionation observed over a 15°C temperature range, two different nitrogenase isoforms, and different organic carbon substrates (succinate, suc.; acetate, ac.; suc.‡ = acidified) is relatively small. The table shows the mean ± SE (n). Individual datapoints, including product and substrate isotopic compositions, are shown in the S.I. Table.

	Temperature	C substrate	$^{13}\alpha_{CO2/CH4}$	$^{13}\varepsilon_{CO2/CH4}$	^{13}n	$^{2}\alpha_{H2O/CH4}$	$^{2}\varepsilon_{H2O/CH4}$	^{2}n
Fe-only nitrogenase	14°C	Suc.	1.061 ± 0.001	61.3 ± 0.3‰	3	2.193 ± 0.004	1193 ± 4‰	3
	19°C	Suc.	1.054 ± 0.001	53.7 ± 1.0‰	12	2.063 ± 0.024	1063 ± 24‰	16
		Suc.‡	1.056	56.3‰	1	2.159	1159‰	1
		Ac.	1.060 ± 0.001	59.6 ± 1.0‰	3	2.064 ± 0.055	1064 ± 55‰	3
	30°C	Suc.	1.049 ± 0.001	49.3 ± 0.6‰	3	2.033 ± 0.030	1033 ± 30‰	3
	All conditions		1.055 ± 0.001	55.1 ± 1.0‰	22	2.078 ± 0.018	1078 ± 18‰	26
V-nitrogenase	19°C	Suc.	1.051 ± 0.002	51.4 ± 2.3‰	3	2.071 ± 0.014	1071 ± 14‰	5